In summary, we have discussed two classes of atomic manipulation processes with the STM and the mechanisms by which they are thought to work. Our understanding of certain mechanisms (for example, electromigration), and whether they constitute a correct explanation of the observed behavior, is clearly in its infancy. We anticipate that this situation will improve as an increasing body of data from different laboratories becomes available. These manipulation capabilities (which are also clearly in their infancy) are already being applied as a laboratory tools, and numerous applications are both fruitful and imminent.

REFERENCES AND NOTES

1. For a review of the STM, see P. K. Hansma and J. Tersoff, *J. Appl. Phys.* **61**, R1 (1987).
2. Two reviews of surface modification with the STM are in press: U. Staufer, in *Scanning Tunneling Microscopy II*, H.-J. Güntherodt and R. Wiesendanger, Eds. (Springer, Berlin, in press); and C. F. Quate, in *Proceedings of the NATO Science Forum '90*, L. Esaki, Ed. (Plenum, New York, in press).
3. R. P. Feynman, *Eng. Sci.* **1960**, 22 (February 1960).
4. E. W. Muller and T. T. Tsong, *Field Ion Microscopy* (American Elsevier, New York, 1969).
5. T. T. Tsong and G. Kellogg, *Phys. Rev. B* **12**, 1343 (1975).
6. S. C. Wang and T. T. Tsong, *ibid.* **26**, 6470 (1982).
7. E. V. Klimenko and A. G. Naumovets, *Sov. Phys. Solid State* **13**, 25 (1971); *ibid.* **15**, 2181 (1974).
8. L. J. Whitman, J. A. Stroscio, R. A. Dragoset, R. J. Celotta, *Science* **251**, 1206 (1991).
9. P. N. First, R. A. Dragoset, J. A. Stroscio, R. J. Celotta, *J. Vac. Sci. Technol. A* 7, 2868 (1989).
10. L. J. Whitman, J. A. Stroscio, R. A. Dragoset, R. J. Celotta, *Phys. Rev. Lett.* **66**, 1338 (1991).
11. D. Heskett, N. J. DiNardo, E. W. Plummer, *J. Vac. Sci. Technol. B* 7, 915 (1989).
12. J. Hebenstreit, M. Heinemann, M. Scheffler, *Phys. Rev. Lett.* **67**, 1031 (1991).
13. M. Krauss and W. J. Stevens, *J. Chem. Phys.* **93**, 8915 (1990).
14. The interaction between the adsorbate and the tip may have components due to the electric field and the tunnel current that under some circumstances could play an important role in the sliding process. The motion of Xe on Ni(110) in the sliding process that we have used is not sensitive to the sign or the magnitude of the electric field, the voltage, or the current. It is only dependent upon the separation of the tip from the adsorbate, from which we deduce that the bonding force is the dominant interaction between the adsorbate and the tip. We find similar results for sliding Pt adatoms and for adsorbed CO molecules (D. M. Eigler, unpublished results).
15. It is also possible to push atoms with the sliding process by simply bringing the tip close enough to the adsorbate so as to operate on the repulsive part of the adsorbate-tip interaction curve.
16. D. M. Eigler and E. K. Schweizer, *Nature* **344**, 524 (1990).
17. *New Sci.* **129**, 20 (23 February 1991).
18. P. F. Schewe, Ed., *Physics News in 1990* (American Institute of Physics, New York, 1990), p. 73 and cover.
19. D. M. Eigler, unpublished data.
20. P. Zeppenfeld, D. M. Eigler, C. P. Lutz, in preparation.
21. D. M. Eigler, C. P. Lutz, W. E. Rudge, *Nature* **352**, 600 (1991).
22. R. Gomer, *IBM J. Res. Dev.* **30**, 428 (1986).
23. T. T. Tsong, unpublished results.
24. R. S. Becker, J. A. Golovchenko, B. S. Swartzentruber, *Nature* **325**, 419 (1987).
25. H. J. Mamin, P. H. Guethner, D. Rugar, *Phys. Rev. Lett.* **65**, 2418 (1990).
26. D. W. Abraham, H. J. Mamin, E. Ganz, J. Clarke, *IBM J. Res. Dev.* **30**, 492 (1986).
27. D. Cleary, *New Sci.* **129**, 31 (26 January 1991).
28. Hitachi, Ltd., press release (14 January 1991).
29. I.-W. Lyo and P. Avouris, *Science* **253**, 173 (1991).
30. A. H. Verbruggen, *IBM J. Res. Dev.* **32**, 93 (1988).
31. K. S. Ralls, D. C. Ralph, R. A. Buhrman, *Phys. Rev. B* **40**, 11561 (1989).
32. Y. J. Chabal, *Surf. Sci. Rep.* **8**, 211 (1988), and references therein.
33. CO bonds to the Pt(111) surface with the C atom closest to the surface and the axis of the molecule normal to the surface. Therefore the molecule appears cylindrically symmetric in STM images.
34. The reader is left to ponder (as do we) what changes occur in the electronic structure that make bridge-bonded CO appear so different from on-top CO.

New Quantum Structures

MANI SUNDARAM, SCOTT A. CHALMERS, PETER F. HOPKINS, ARTHUR C. GOSSARD

Structures in which electrons are confined to move in two dimensions (quantum wells) have led to new physical discoveries and technological applications. Modification of these structures to confine the electrons to one dimension (quantum wires) or release them in the third dimension, are predicted to lead to new electrical and optical properties. This article discusses techniques to make quantum wires, and quantum wells of controlled size and shape, from compound semiconductor materials, and describes some of the properties of these structures.

THERE HAS BEEN SWIFT PROGRESS IN RECENT YEARS IN THE synthesis of artificial quantized structures. Electrons in these small structures show quantum effects that strongly modify their behavior. Progress has been especially rapid in layered quantum structures (*1*), which are stacks of precisely deposited thin films in which electrons show fundamentally new electrical and optical properties. These materials offer a miniature laboratory that has influenced our basic understanding of solids and has provided new kinds of optical and electronic devices (*2*). Among the discoveries emerging from layered structures are the quantum Hall effect (*3*) (for which the 1985 Nobel Prize in Physics was awarded), transistors with record speed, and lasers with record low threshold currents for lasing. Practical application of the structures has been so rapid that they are encountered now in our daily lives. Devices currently being manufactured with layered quantum structures include most lasers in compact disc players, low noise amplifiers in direct broadcast satellite receivers, and laser sources for fiber optic communication.

Past research on quantized semiconductor structures has focused on layered structures that confine conduction electrons to two dimensions. Now, systems in which the electrons are confined to one dimension of free motion (quantum wires) are providing materials with remarkable new properties [for instance, the quantization of electrical conductance in ballistic quantum wire channels (*4*)]. But the challenges of fabricating these wire-like structures are greater than those for making layered structures, and extensive improvements in the fabrication techniques are needed. A starting point for the fabrication of quantum wires has often been two-dimensional layered structures that are lithographically processed to achieve lateral confinement. But higher performance will require the fabrication of smaller structures for which it will probably be necessary to actually control the lateral motion of atoms during growth of the materials. This presents a major challenge in growth technology for the next generation of quantum structures.

The authors are in the Department of Electrical and Computer Engineering, and Materials Department of the University of California, Santa Barbara, CA 93106.

Another class of quantized semiconductor structures in which new and previously unattainable phenomena are now being observed is provided by materials with wider layers in which electrons have a third degree of freedom. These materials provide an approach to a three-dimensional electron gas for which new ordered states of the electrons have been predicted and for which new behaviors in the far infrared and submillimeter wave spectral region may be investigated.

The majority of the structures discussed above have been fabricated using III-V compound semiconductors. These materials are compounds of elements from the third column (group III) and elements from the fifth column (group V) of the periodic table. Gallium arsenide (GaAs) and aluminum arsenide (AlAs) have been the two most intensely studied III-V compound semiconductors. In this article we present the design concepts, growth, and properties of the new quantized structures in the III-V compound semiconductor system.

Two-Dimensional Electron Systems—Background

The fundamental design concept that enables quantized electron structures to function is the difference in electron affinity between different materials. For example, a conduction electron has greater affinity for GaAs than for AlAs. When introduced into a stack of layers of GaAs and AlAs (called a heterostructure, as opposed to a homostructure which consists of a single type of semiconductor), the electron prefers to be in the GaAs layers, it being energetically favorable to do so. An electron is thus confined in a square potential well created by a layer of GaAs sandwiched between two layers of AlAs (Fig. 1a).

The depth of the well can be varied over a range of about 500 meV, for example by employing an alloy of AlAs and GaAs ($Al_xGa_{1-x}As$, where x is the Al mole fraction) rather than just pure AlAs, for the barrier layers. The well-depth is proportional to the difference between the bandgaps of the barrier and well layers, and varies almost linearly with x, for x ranging from 0 to 0.45. With well-controlled epitaxial growth techniques (*5*) like molecular beam epitaxy (MBE) and metal-organic chemical vapor deposition (MOCVD), it is now possible to grow layered ultrahigh purity thin single-crystalline films of compound semiconductors, where the thickness of each layer can be precisely controlled down to a single layer of atoms (approximately a few angstroms thick). This control over the well depth and the well thickness enables one to engineer the microscopic operating environment for electrons in quantum structures.

As explained in basic quantum mechanics textbooks, the allowed energy states of an electron are discrete or quantized. The energy of an electron confined in a potential well that is formed by a layer of GaAs sandwiched between two layers of $Al_xGa_{1-x}As$ is similarly quantized (Fig. 1a). The difference in energy between two quantized levels becomes larger when the width of this potential well is reduced. This difference becomes of practical use in GaAs/AlAs heterostructures when the width of the GaAs layer is reduced to less than a few hundred angstroms. It is important to bear in mind, though, that the potential well produced in the manner described above confines the electron only in one direction, namely the growth direction. The electron is essentially free in the plane of the substrate (the wafer, usually GaAs, on which the GaAs/AlAs thin film stack is grown). Hence the name: the two-dimensional electron gas or 2DEG. The electrons in this gas are distributed in a set of energy subbands, in which the bottom (the lowest energy state) of each subband is determined by the energy quantization in the growth direction; the higher energy values within each subband arise from the kinetic energy of the electrons in the substrate plane.

The electrons themselves are introduced by the technique of doping: a donor impurity such as Si is used to dope either all the layers or just selective layers [the latter technique is called modulation doping (*6*)]. In the AlGaAs system the group IV Si atom is incorporated substitutionally onto a group III Al or Ga site, donating its extra valence electron for conduction. When only the $Al_xGa_{1-x}As$ layers are modulation doped, the electrons fall into the neighboring potential wells and are spatially separated from the parent ionized donor atoms in the barriers. As a consequence, the scattering of the electrons by the donor atoms is drastically reduced. The benefits of this reduction are most strongly realized at liquid helium temperatures when the scattering from lattice vibrations is frozen out, and the electrons enjoy large mean free paths (the average distance the electrons travel between collisions) in the plane of the quantum well. Low-temperature electron mobilities (electron drift velocity per unit of applied electric field) in excess of 10 million $cm^2 V^{-1} s^{-1}$ have been reported in the last 2 years (7). Such mobilities and their attendant large mean free paths have enabled the discoveries of new phenomena attributed to electron-electron interactions, such as the fractional quantum Hall effect (*8*) in high-purity low-disorder systems, and have prompted an intense search for the 2D Wigner crystal, the lattice which the electrons are predicted to freeze into in the limit of absolute zero temperature ($T = 0$ K) (*9*).

High-speed electronic devices such as the high electron mobility transistor (HEMT) and the heterojunction bipolar transistor (HBT), and optical devices such as lasers, are some of the practical applications of bandgap-engineered 2D electron systems (*10*). The

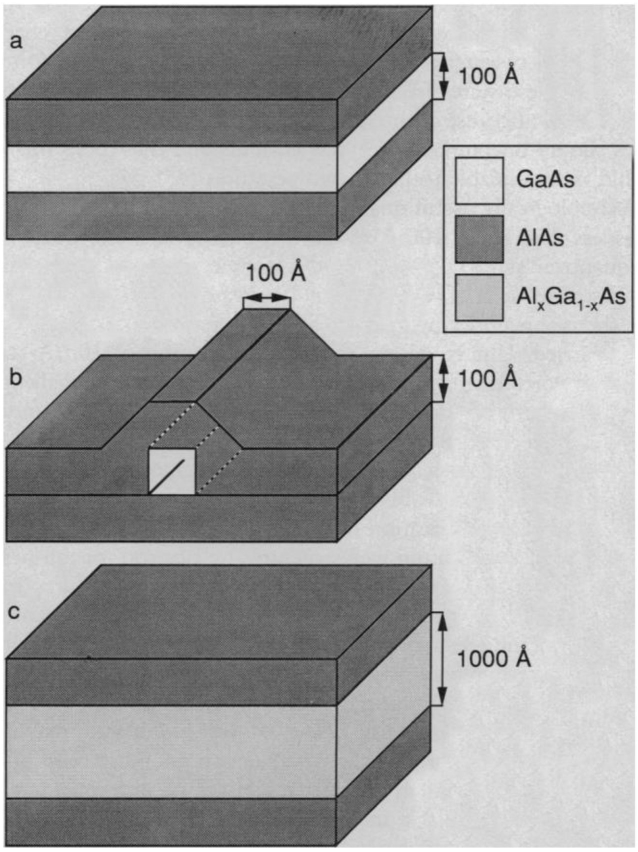

Fig. 1. Schematic sketch of layered quantized structures used to confine electrons and fabricated from stacks of precisely deposited thin films of GaAs and AlAs. (**a**) Quantum well that confines electrons to two dimensions. (**b**) Quantum wire that confines electrons to one dimension. (**c**) Wide specially shaped quantum wells that can be used to study effects of weakening confinement in the vertical direction.

high electron mobility resulting from modulation doping, and the consequent fast electron transport between source and drain of a field effect transistor, gives the fast switching speed and high-frequency operation of the HEMT (*11*). The emitter gain of a n-p-n HBT is increased by using a larger bandgap material for the emitter than for the base, which enhances electron flow from emitter to base, while at the same time inhibiting the backflow of holes from base to emitter (*12*). Heterostructure lasers employ larger bandgap materials in the p and n regions of a p-i-n diode, which serve to provide not only electrical confinement of electrons and holes in the lower bandgap i (intrinsic or undoped) region into which they are electrically or optically pumped, but also optical confinement of the lasing mode resulting from radiative recombination of the injected electrons and holes (*13*).

Approaches to One-Dimensional Structures

Fundamental new features are expected when electrons are further confined into quantum wires, so that their only degree of free motion is along the wire (Fig. 1b). The effects of scattering on electron motion are greatly changed in this case. In two and three dimensions, most of the scattering of electrons occurs by small deflections, or small-angle scattering. In quantum wires, however, this scattering is strongly reduced, and 180° direction reversals become the only energy-conserving collisions that are allowed (*14*). Recently, it was found that electrical conductance in ballistic wires, which are wires shorter than the electron mean free path so that electrons move in ballistic trajectories, become quantized in integral units of e^2/h (*4*). Energy quantization effects become even more dominant than in two dimensions, with the increased energy separation between the electron states and the redistribution in energy of these states from the constant distribution for 2D into peaks for 1D. Because of this, semiconductor lasers in ideal quantum wires should operate at lower bias currents and their performance should be sustainable to higher temperatures (*15*).

Technologically useful quantum wires will require lateral dimensions less than about 100 Å so that the energy separation between the quantized states ($E_n \sim n^2h^2/8m^*L^2$ for electrons of effective mass m^* in square wells of width L) will be greater than room temperature thermal energies, which will allow appreciable device currents to be carried. Unfortunately, precision fabrication of 100 Å scale quantum wires is proving to be a difficult technological challenge. Several methods are currently being pursued to fabricate quantum wires; all these methods use the more conventional epitaxial techniques mentioned earlier in at least some capacity (Fig. 2).

Probably the most obvious and the most common method attempted for the fabrication of 1D structures is the processing of conventional 2D quantum well structures by electron- or ion-beam writing techniques (Fig. 2a); typical processing procedures may include damaging or removing undesired regions of the quantum well, or patterning evaporated metal gates on its surface to electrically deplete certain regions. These techniques have the advantage of being very flexible with respect to the patterned features. With the use of high electron mobility 2D structures as substrate material, these structures have probed the wavelike nature of electrons in the ballistic electron transport regime. Examples of new phenomena discovered by this work include the quantized conductance of ballistic wires (*4*) as mentioned above, electron optics in semiconductors (*16*), and varied magnetic phase interference (*17*). Unfortunately, although features as small as 15 Å have been produced in other materials, the effective resolution of these techniques in semiconductors is at best about 300 Å because of difficulties involved with transferring patterns to the semiconductor materials and with surface damage effects. The energy quantization effects attributable to these lateral sizes are not large compared to thermal energies at room temperature. Therefore these techniques are not presently capable of producing 1D structures that will operate above cryogenic temperatures.

A recent approach, in which conventional epitaxy is used to form 1D structures, involves cleaving a conventional 2D quantum well structure to form an edge that is perpendicular to the original layers (Fig. 2b). This cross-sectional edge is then used as a new surface to grow a second confinement layer (*18*). This technique is exciting because of its potential for producing small-scale 1D structures for study, but structures that exhibit 1D properties have yet to be reported. Before commercial device application becomes feasible, the challenges related to the very small active areas on the edge of the cleave and the number of procedures it takes to make the structures, must be overcome.

One-dimensional structures can also be formed by epitaxially depositing atoms on prepatterned substrates (Fig. 2c) (*19*). The substrates are typically etched by conventional wet chemical methods so that they have an array of V-shaped grooves that are typically about 5000 Å wide and deep. When a thin layer of GaAs is deposited on this surface, the atoms preferentially migrate to the bottom of the grooves, forming a narrow crescent shaped quantum well, on top of which is grown an AlGaAs barrier layer. Lateral motion of atoms on the growth surface is thus used for wire formation. This leads to a structure with an effective lateral confinement of somewhat less than 1000 Å in width. Lasers have been made from this type of structure, but because of the relatively large lateral size, performance enhancement due to the additional confinement has been small.

A fundamentally different fabrication method that also relies on the motion of atoms on the growth surface, but has the potential to make smaller quantum wire structures (periods of less than 80 Å have been obtained), makes use of atomic steps on a crystal surface (Fig. 2d) (*20*). The atomic steps allow some control over the lateral placement of the atoms deposited on the crystal surface, and the formation of 1D structures without having to resort to intermediate processing steps or patterned substrates. For these reasons, our effort at UCSB in the growth of quantum wires has focused on this

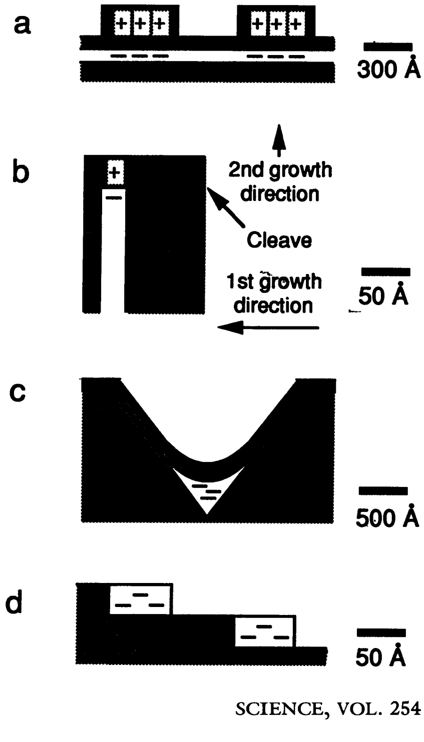

Fig. 2. Schematic illustrations of various methods being developed to fabricate quantum wire structures (vertical dimensions not to scale). (**a**) Patterning the surface of a conventional 2D quantum well by focused ion beam or electron beam. (**b**) Cleaved edge overgrowth, which forms a 1D structure by growth on the cleaved edge of a conventionally grown 2D quantum well. (**c**) Overgrowth of prepatterned V-grooved substrates. (**d**) Formation of a lateral superlattice (LSL) by growth on atomically-stepped substrate.

technique. Like the methods described above, this technique shows promise for ultimately producing high-quality 1D structures, but it too is an immature technology.

The semiconductors on which epitaxial layers are grown are crystals composed of periodic, closely spaced atomic planes. Normally, growth is performed on a surface that is cut parallel to one of the primary crystallographic planes (Fig. 3a), but if the orientation of the cut is instead slightly away from such a plane, the surface will intersect the primary atomic planes at regular intervals, resulting in a periodically stepped surface (Fig. 3b). The period, or width, of the steps depends on the angle the surface is misoriented away from the primary plane; for example, a surface tilted 2° from the GaAs (100) plane has steps with an average spacing of about 80 Å. These steps can then be used to create lateral structures with the same period, as discussed below. Under the correct growth conditions (such as substrate temperature and source fluxes), the deposited atoms can be made to position themselves at the step edges, where more atomic bonds are available per bonding site than on the step terraces. This results in a stronger bond between the deposited atoms and the substrate. If all the deposited atoms have enough thermal energy to migrate to a step edge and adhere there before bonding somewhere on the terrace, growth occurs by the propagation of the step edges, a process known as step-flow growth. The thermal energy for atom surface migration is provided by the substrate, which, in the case of GaAs growth, is typically heated to about 600°C throughout the growth. Higher substrate temperatures provide more thermal energy, resulting in larger atom surface migration lengths, and therefore a better chance for step-flow growth to occur.

Step-flow growth is important because it allows atoms to be placed on a surface in an ordered manner. To use it to form structures with very small lateral dimensions, enough material of one compound (such as GaAs) is deposited to cover a fraction of each of the step terraces (that is, deposit a fraction of a monolayer) (Fig. 3c), and then enough material of a second compound (such as AlAs) is deposited to cover the remaining area of the terraces (Fig. 3d). Because growth is by step-flow, the first compound will cover the back portion of the terraces, while the second will cover the front portion; if, during this process, exactly one monolayer of material is deposited, the step edges return to their original locations. The result is a lateral structure that has a very short lateral period and that is one monolayer thick (~3 Å). To produce a thicker structure, this process is simply repeated as many times as necessary, stacking regions of like-compounds on top of each other, creating a lateral superlattice (LSL) (Fig. 3e). This structure can be used to confine electrons lateral to the growth surface, and can be used in combination with conventional layer growth techniques to produce 1D structures. A common name for these LSLs is tilted superlattices, because if a total of slightly more or less than one monolayer is deposited each cycle, the step edges will not return to their original locations. This causes the regions of like compounds to stack slightly displaced from the previous layer deposited, and thereby results in tilted stacks of compounds (Fig. 3f) (*21*). Lateral superlattices have been successfully grown in both the AlAs/GaAs material system (*21, 22*), and the similar AlSb/GaSb material system (*23*). The change of the LSL tilt with deposition amount per cycle can be directly seen and measured by cross-sectional transmission electron microscopy (TEM) (Fig. 4). With present deposition systems it is difficult to control the deposited amounts to better than about 1 to 2%, which can lead to tilt uncertainties as great as 30°. This lack of control over LSL tilt is undesirable because it leads to uncertainties in the confinement widths of the LSLs and hence in the quantized electron energy levels. It should be possible to design the next generation of MBE equipment to have improved control over deposition quantities, but until this capability is available, we will have to rely on clever structural designs to consistently grow untilted, or vertical, LSLs.

One way to guarantee a confinement region that will contain a vertical LSL is to grow what is known as a serpentine superlattice (SSL) (*24*), which is a LSL whose deposition amounts, and therefore whose tilt, is varied continuously from the bottom of the structure to the top. If, for example, the deposition amount per cycle is raised from 0.95 to 1.05 through the SSL growth, then the SSL tilt will vary continuously between about +70° and −70°. The SSL thereby contains a region in which the deposition per cycle is one monolayer and the barrier regions are vertical. In this way small uncertainties in the deposition rate will affect the beginning and final tilts, but an intermediate vertical region is guaranteed. Because the wells in the vertical region are wider than those in the tilted regions,

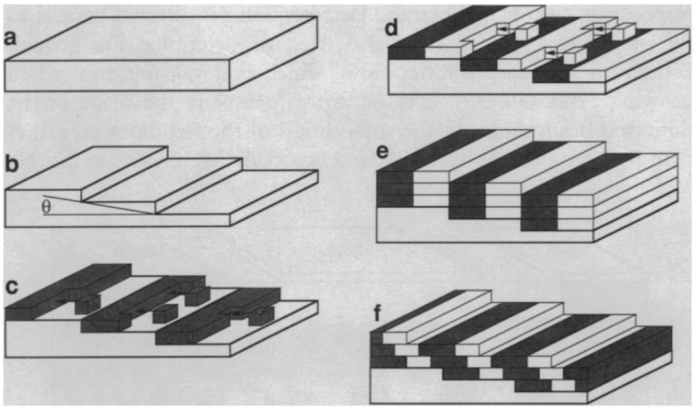

Fig. 3. (**a**) Nominally flat crystal surface, which is cut parallel to a primary crystal plane [usually (100)], and is used for the majority of epitaxial growths. (**b**) Atomically stepped crystal surface, produced by cutting a crystal at an angle θ from a primary plane. (**c**) The first step in forming a LSL: deposition of enough material of a compound to cover a fraction of each step terrace. Because of stronger bonds there, deposited atoms prefer to adhere to the step edges, causing these edges to propagate across the step terraces. (**d**) The second step in forming a LSL: deposition of a second compound to cover the remaining portions of the step terraces. If the total amounts of the two compounds deposited sums to exactly one monolayer, then the step edges will return to their original locations. (**e**) Formation of a thicker LSL by repeating the steps in (c) and (d). (**f**) Formation of a tilted LSL by depositing a sum of less than a monolayer of material each deposition cycle.

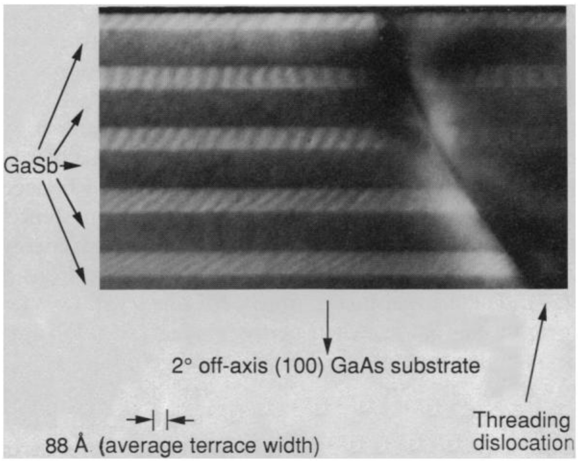

Fig. 4. Cross-sectional transmission electron micrograph of four AlSb/GaSb lateral superlattices, formed by depositing nominally 0.4 monolayers of AlSb followed by 0.6 monolayers of GaSb in each of 40 deposition cycles per LSL. The LSLs are separated by layers of GaSb, and they differ in the amount they are tilted, which is caused by each LSL having a different sum of AlSb and GaSb deposited each cycle. The sums for the layers are, from top to bottom, 1.00, 1.01, 1.03, 1.05.

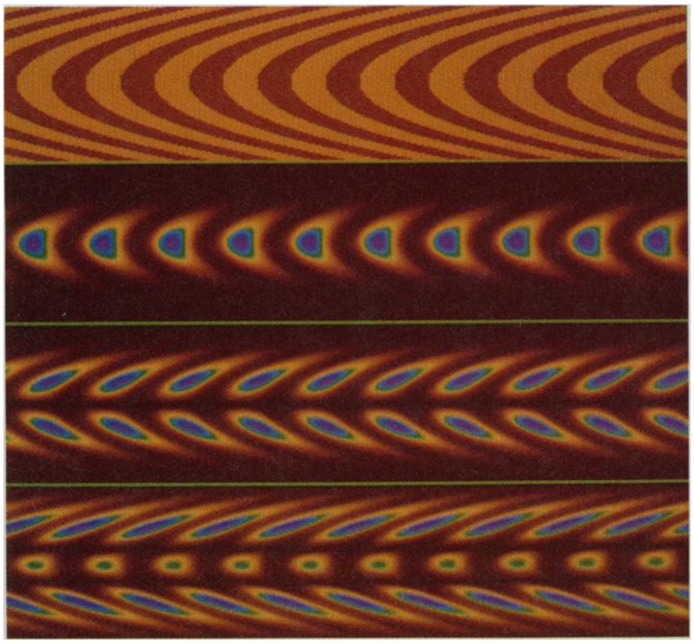

Fig. 5. Top section: schematic diagram of a serpentine superlattice (SSL), where the dark regions are AlAs barriers and the light regions are GaAs wells. Bottom three sections: the calculated three lowest energy electron wavefunctions for the SSL shown, with the ground state in top, followed by increasing energy states. Brightest regions indicate maximum electron density, dark regions denote zero electron density. The ground state has a density maximum at the SSL center, indicating 1D confinement. Higher energy states are less well confined.

electrons will have lower confinement energies and be more concentrated there, resulting in a well-controlled 1D structure. Calculations of the three lowest energy electron wavefunctions in such a structure indicate that the ground-state wavefunction has density peaks at the center of the structure, showing the 1D nature of the electrons (Fig. 5). Successive wavefunctions, which have increasingly higher electron energies, are less well confined.

While TEM images give visual evidence of the successful formation of LSLs, there are also a number of electrical and optical experiments that have supplied information on the nature of the lateral electron confinement the LSLs provide. For example, one monolayer thick LSLs imbedded in AlGaAs/GaAs 2D structures have resulted in devices that exhibit electron mobility anisotropies where the electrons are more free to move in the direction parallel to the LSLs (*25*). AlGaAs/GaAs HEMT structures with LSLs at the conducting interface (Fig. 6) (so-called washboard transistors) have also been demonstrated (*26*). These transistors exhibit a new kind of transistor action owing to a switchable interference between the conduction electrons and the LSL (*26*). Photoluminescence from LSL structures show polarization dependencies and energy-level shifts that are due to the lateral redistribution of electrons by the LSLs (*27*). These experiments were performed with simple LSL structures; in the future, when perfected, the LSL technique will allow for a wide range of possible structural geometries.

Although the above experiments suggest that LSLs are indeed modifying the electron distribution lateral to the growth plane, they have also shown that complete lateral confinement is not occurring; that is, electrons to a significant degree are able to move between different columns of the LSLs, and the structures are therefore not truly 1D. The causes of this have been attributed to two ways in which the LSL structures deviate from ideal behavior, both of which are related to their growth. One is the nonuniformity of the stepped surface, which causes the confinement regions to vary in width laterally across the sample. Consequently, the electron confinement energies and the amount of tunneling between the 1D structures also varies. The other is the intermixing that occurs between the two compounds of the LSL. Intermixing results in a reduction of the energy barrier heights between the 1D structures. The resulting spread in electron energies in the structures also reduces their usefulness in many applications, for example "single wavelength" lasers with narrow wavelength distributions.

The most common technique for determining LSL uniformity is cross-sectional TEM, which gives a side view of the LSL (Fig. 4). This view provides direct information on the widths of the terraces, the LSL tilt orientation, and compound intermixing. To get an idea of the uniformity in the growth plane, however, we need a top view of the LSL. This can be acquired by using planview TEM through a thinned sample. The image obtained is accurate only if the LSL is vertically oriented which, unfortunately, is often not the case. An alternative method for viewing the LSL structure from the top uses atomic force microscopy (AFM) to detect GaAs ridges that are left behind on a surface LSL after the AlAs regions have been chemically etched away (*28*). AFM can produce a perspective view of these ridges (Fig. 7). This method can be extended to image large surface areas of the LSLs, thereby determining their degree of nonuniformity.

Ideally, we would like to grow LSLs on surfaces with straight and uniformly spaced step edges. To prepare the stepped substrates, wafers are first cut from a crystal ingot so that they have the desired surface orientation, and are then mechanically and chemically polished to remove as much of the surface roughness as possible, because surface roughness results in a nonuniform distribution of step terrace widths. This surface roughness can be investigated with reflection high-energy electron diffraction (RHEED). RHEED is an important MBE tool which, among other things, can be used to monitor the evolution of the terrace widths while growth is taking place. It consists of analyzing high-energy electrons (~10 keV) that have been reflected from the sample surface at a low incident angle, typically 1 to 2 degrees from the surface plane (*29*). In this geometry the electrons are sensitive to the arrangement of essentially the top layer or two of atoms. When the beam is directed down the surface steps, the periodic steps result in a series of diffracted electron beams, and from their spacing and shape we can deduce the step periodicity and terrace width uniformity, respectively (*30, 31*). When the electron beam is directed parallel to the step edges, RHEED is also used to determine the growth conditions necessary for step-flow, which is a valuable tool when growing LSLs (*30, 32*), because in this geometry the shape of the diffracted beam measures the smoothness of the step terraces, rather than the step periodicity. MBE and especially MOCVD can quickly

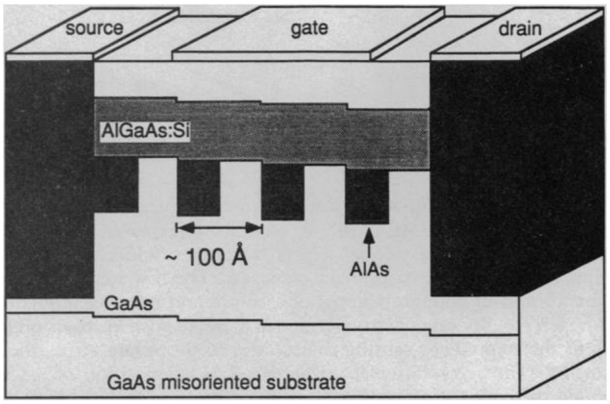

Fig. 6. Cross section of an AlGaAs/GaAs HEMT device with a LSL immersed in the 2DEG at the conducting interface (so-called washboard transistor). By tuning the electron density with the gate, switching due to interference between the conduction electrons and the LSL can be achieved (*26*).

smooth the individual terraces, but the unequal terrace widths that result from the nonflat surface heal more slowly, especially for long-range roughness variations. Experimentally, a 3000 Å buffer layer grown on top of an as-polished substrate can reduce the standard deviation of the terrace width fluctuations (which we assume are roughly Gaussian distributed) from on the order of several terrace widths to about half a terrace width, as measured by cross-sectional TEM and in situ RHEED (*30*). Unfortunately, this remains a significant nonuniformity.

A topic of current research and possibly the most serious obstacle in LSL development is the intermixing of the LSL's two constituent compounds during growth. This intermixing raises the energy of electrons in the wells, lowers the energy of the barriers, and effectively reduces the 1D nature of the LSLs. The intermixing can be caused by the thermal diffusion of the deposited atoms from their desired positions. Unfortunately, the same hot substrate that is necessary for step-flow growth causes this thermal diffusion. Thus, LSL growth involves a trade-off: at too low a substrate temperature the deposited atoms cannot all reach the step edges, while at higher substrate temperatures there is increased intermixing. With present growth techniques, there appears to be no position in the temperature window for GaAs/AlAs LSL growth that allows for completely segregated well and barrier regions. Current research of segregated LSL growth is focused on lowering the temperature necessary for atoms to reach the step edges. This can be attempted by optimizing conventional growth conditions such as the group III atom deposition rates and the ratio of the two compounds in the structure. It can also be accomplished by a technique known as alternating-beam, or migration-enhanced epitaxy (*33*). This method entails depositing the group V atoms of a layer after the group III atoms; this results in greater migration lengths for the group III atoms as they have more time to move around before combining with the group V atoms to form the final compound. This technique can be used for one or both of the compounds of the LSL, and results in a reduction of the minimum step-flow temperature (by about 20 to 30°C in AlAs/GaAs LSLs) (*34*), and a better, though not perfect, LSL segregation. For drastic improvements in LSL segregation it may be necessary to resort to nonconventional growth techniques, such as using a nonthermal energy source (such as light or particle beams), which would allow us to selectively excite migrating atoms, but not atoms already in their desired positions.

Although further advances in epitaxial technology should allow for improved growth of LSL structures, perfect segregation of LSL components may not be necessary for many applications. In any event, growth of LSL structures is revealing a great deal about atomic motion and growth on atomically stepped surfaces, and about the physics of low-dimensional structures.

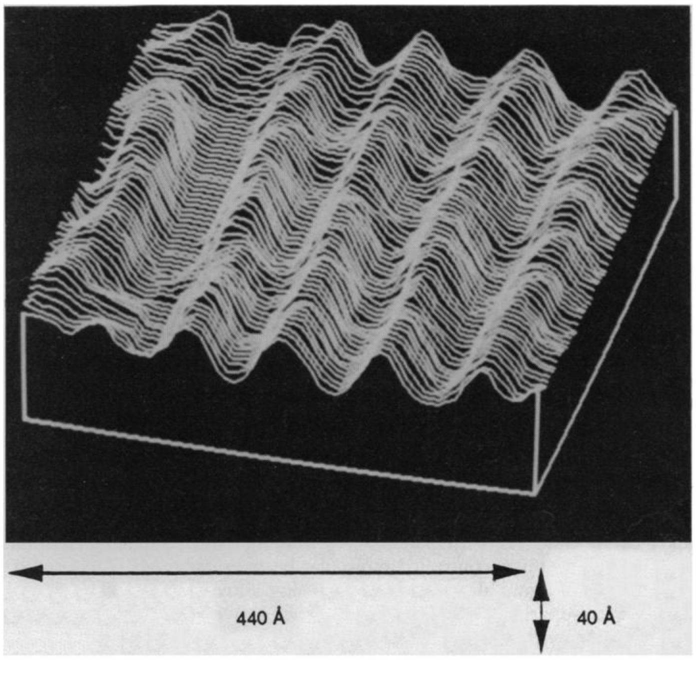

Fig. 7. Atomic force microscope image of lateral superlattice structure. GaAs ridges are formed after the AlAs columns of an AlAs/GaAs surface LSL are chemically removed. This technique can be used to study LSL uniformity in the growth plane.

Approaches to Three-Dimensional Structures

Advancement of the research on electron systems has been predominantly toward more confinement—from quantum well (2 degrees of freedom) to quantum wire (1 degree of freedom) to quantum box (0 degrees of freedom). Surprisingly, no comparable effort has been undertaken in the opposite direction, that is in the study of high-quality three-dimensional (3D) systems (Fig. 1c) in which the conduction electrons have 3 degrees of freedom. Although there has been extensive research in the study of high electron density 3D systems such as metals, our understanding of low-density 3D systems such as semiconductor structures is rather poor. There are several interesting but as yet unverified predictions for low-density 3D electron systems. For instance, in the limit of zero temperature and in sufficiently strong magnetic fields, a low-density electron gas is predicted to undergo a

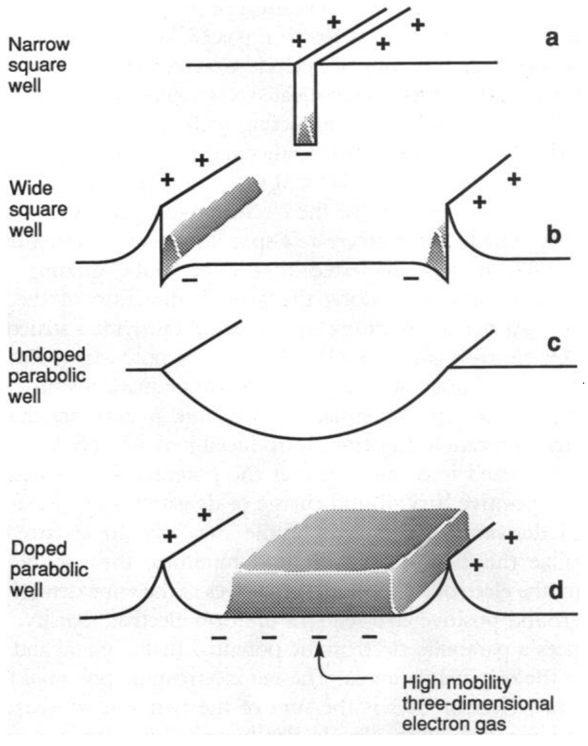

Fig. 8. Schematic of different potential energy wells for four different heterostructures, and the electron distributions (shaded) within each. The barriers surrounding the potential well are doped in order to supply electrons to the well. For a narrow square well (**a**), the electrons are concentrated at the well center. For a wide square well (**b**), the electrons repel each other and accumulate at the two interfaces. To obtain an electron gas with uniform density, the well must be graded parabolically (**c**) to compensate for this electrostatic repulsion. From Poisson's equation, electrons introduced into a parabolic well by doping the barriers (**d**) distribute themselves uniformly at a density given by the curvature of the parabola.

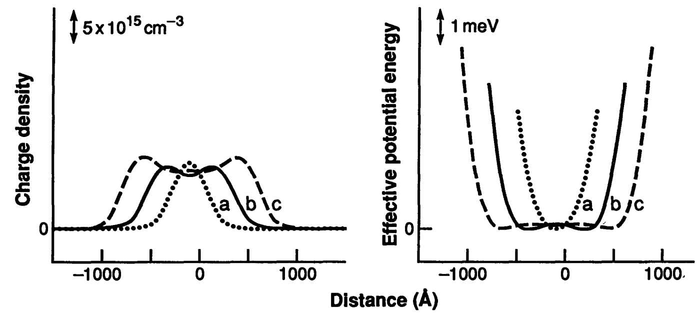

Fig. 9. Electron distribution (left) and effective potential energy (right) versus distance as the number of electrons in the parabolic well is increased. Curve a corresponds to the case when only one subband is occupied; curve b, two subbands occupied; and curve c, three. Note that the height of the charge density distributions, on the left, is preserved from curve a through curve c. The increasing thickness of the distribution accommodates the increase in the number of electrons. Note also the flattening, on the right, of the parabolic well over the region of occupation of the electrons. This flattened portion increases from curve a through curve c with increasing thickness of the electron distribution.

transition to a spin-density wave state (*35*), where the electron-electron interaction causes spin ordering in the ground (lowest energy) state, producing highly anisotropic electrical properties. In still stronger magnetic fields or at lower electron densities, the electron gas is predicted to form a 3D Wigner crystal. One would expect a uniformly doped semiconductor (such as GaAs doped with Si) to be a sufficient candidate for this study. But the semiconductor electron gas floats in a sea of fixed discrete background charges (of the donor ions). Electron scattering from the donor atoms inhibits observation of many effects expected for an ideal three-dimensional electron gas (3DEG).

One might expect to obtain thick electron layers of high mobility by using modulation-doped wide square wells in which the dopant atoms lie exclusively outside the conducting well channel. However, the charged electrons will repel each other and form two narrow electron layers near the walls (the GaAs/$Al_xGa_{1-x}As$ interfaces) of the well (Fig. 8b). Compensation for the electrostatic repulsion between the electrons must be made to create a spatially uniform 3DEG density.

In 1987, it was suggested that a parabolic grading of the conduction band edge along the growth direction of the GaAs/$Al_xGa_{1-x}As$ heterostructure (Fig. 8c) would provide a structure for a thicker electron gas layer (*36*). A parabolic potential is equivalent to a constant charge, according to Poisson's equation $\nabla^2\Phi = -\rho/\varepsilon$, relating electrostatic potential Φ to charge ρ in a material with dielectric constant ε. Electrons introduced into a parabolic potential well are tricked into thinking that the potential is produced by a uniform positive background charge of density proportional to the second derivative (curvature) of the parabola. In an attempt to neutralize this fictitious charge and minimize the energy of the system, the electrons distribute themselves at the same density as this background positive charge. This uniform electron density in turn produces a parabolic electrostatic potential that is equal and opposite to the original parabola. The net electrostatic potential that an individual electron sees is the sum of the two and consists of the original parabola with a wide flat bottom, the flattened portion being the region where the electrons are sitting (Fig. 8d). This is what one expects classically (*37*).

Quantum mechanical corrections are expected to be important at low temperatures where the separations between the quantized electron energies or subbands are larger than the thermal energy (kT). Owing to the large well width (typically 1000 Å) these subbands are separated by roughly 1 meV, and are larger than the thermal energy only for $T < 10$ K. Despite this energy quantization, quantum mechanical calculations of the electron distribution in a parabolic well at $T = 0$ K show that this distribution is still uniform at the curvature density as long as there is more than one energy level or subband occupied (*38*). In fact, the more subbands that are occupied, the more the gas behaves classically. When only the lowest subband is occupied, the 3D density of the electron distribution increases with increasing number of electrons in the well, as for a 2DEG. As soon as the second subband is occupied, this 3D density is essentially pinned at the curvature value. Addition of more electrons into the well only makes the electron layer thicker (Fig. 9), while retaining a constant 3D density. A few ripples are observed in the distribution due to the finite number of subbands occupied. The number of electrons in these wells can be controlled with a surface gate as in a field-effect-transistor; the electron gas can therefore be tuned to have one, two, three, or more subbands occupied, and its properties can be studied in the transitional regime from 2D (one occupied subband) towards 3D (more than one occupied subband).

This concept is general and can be used to realize carrier profiles of different shapes by introducing electrons into potential wells whose second derivatives are proportional to the desired carrier density distributions, according to Poisson's equation. Classically, in the limit of zero temperature the electron density tracks the curvature of the well exactly; quantum mechanically, the density follows the curvature fairly closely once more than one subband is occupied.

As stated in the introduction, the bandgap of $Al_xGa_{1-x}As$ varies linearly with Al mole fraction x, over a certain range of x. A parabolic potential well in the conduction band for electrons can therefore be realized by synthesizing a graded $Al_xGa_{1-x}As$ alloy with a parabolic mole-fraction profile. Computer-controlled MBE can be used to grow a graded alloy of $Al_xGa_{1-x}As$ with precisely controlled Al mole fraction variation (*39*). This variation can itself be achieved in two ways: by pulsing the Al beam, or by varying the Al flux by controlled variation of the Al oven temperature, in the presence of constant Ga and As fluxes impinging on a GaAs

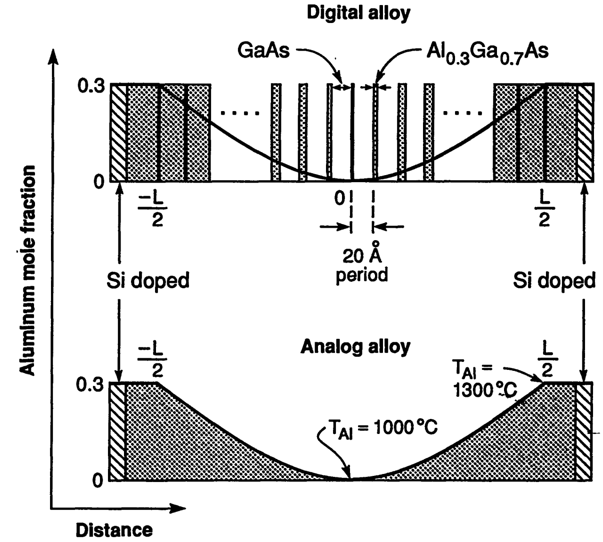

Fig. 10. Realization of a parabolic potential well by synthesis of a graded alloy of $Al_xGa_{1-x}As$ with parabolically varying (with distance) Al mole fraction x. Computer-controlled molecular beam epitaxy (MBE) is used to make either a digital alloy (top) or an analog alloy (bottom). The digital alloy is a superlattice consisting, in the above case, of GaAs and $Al_{0.3}Ga_{0.7}As$, with a 20 Å period; the pulse duration of the $Al_{0.3}Ga_{0.7}As$ is varied parabolically so that the average Al mole fraction versus distance is parabolic (top). The temperature of the Al oven is varied continuously in the presence of constant Ga and As fluxes to obtain the graded analog alloy (bottom). The barriers are doped with Si to supply electrons to the well. The width L of the well is usually between 1000 Å and 6000 Å.

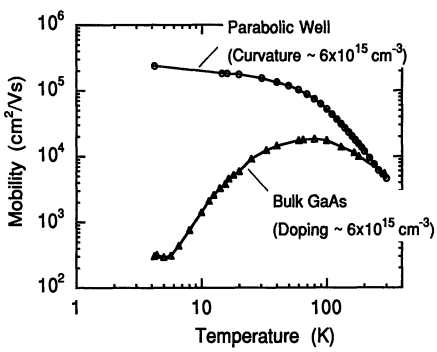

Fig. 11. Electron mobility versus temperature for a 2000 Å thick electron gas in a parabolic well (at the curvature density ~6 × 10^{15} cm^{-3}) and for bulk GaAs uniformly doped at the same density. The spatial separation of the donor atoms in the barriers from the electrons in the well reduces scattering and enhances the mobility of the electron gas in the parabolic well to be over two orders of magnitude higher than for the bulk GaAs at low temperatures. The collision of electrons with the rough walls confining the gas may be the scattering mechanism that limits the in-plane mobility.

substrate (Fig. 10). The former is called a digital alloy, the latter an analog alloy. Parabolic wells have been grown by both techniques and show similar electrical and optical properties.

The digital alloy is essentially a superlattice (a periodic extension of a unit cell that consists of two or more different materials) with a period of typically 20 Å; each period consists of two layers: GaAs and Al$_y$Ga$_{1-y}$As where y is the maximum Al mole fraction in the structure, usually the value in the barriers. The pulse duration of the Al$_y$Ga$_{1-y}$As is varied parabolically by computer control. The 20 Å superlattice period is sufficiently small to permit tunneling of electrons between the layers so that the electron sees an effective average Al mole fraction that varies parabolically with distance (Fig. 10). The parabolic composition profile can be calibrated by Al flux measurements where an ion flux gauge is used in place of the substrate (*40*). The Al mole fraction can be controlled to within 5% of its nominal value and the curvature to within 10% by computer control of the Al oven shutter (for the digital alloy) or the Al oven temperature (for the analog alloy).

The electrons are introduced by selectively doping the barrier layers on either side of the parabolic well with donors such as silicon. As in the case of the 2DEG described earlier, the spatial separation of the electrons from the ionized donors results in a mobility for motion in the substrate plane up to two orders of magnitude higher, at temperatures $T < 100$ K, than would be obtained in a uniformly-doped semiconductor with the same 3D density of electrons (Fig. 11). Mobilities in excess of 100,000 cm^2 V^{-1} s^{-1} (and as high as 350,000 cm^2 V^{-1} s^{-1} for a 3DEG with density ~10^{16} cm^{-3}) have been obtained in a variety of 3DEGs with densities ranging from as low as 4 × 10^{15} cm^{-3} up to 10^{17} cm^{-3} (*41, 42*). Although this mobility is much higher than for uniformly doped materials, it is still substantially lower than the best mobilities in 2DEGs.

Low-temperature transport measurements in a magnetic field show oscillations in the resistance of the gas and the well-known quantum Hall effect (*43*). A Fourier analysis of the oscillations reveals multiple frequencies which are related to the occupation of electrons in individual quantized subbands. This analysis reveals the Fermi energy of the electron gas in the parabolic well to be fairly constant as the number of electrons is changed and is therefore a signature of the three-dimensionality of the gas (in the 3D limit the Fermi energy is constant for a uniform 3D density). The analysis yields the energies as well as the number of electrons in each subband, which agree with calculations to within 10%, an agreement that is rather remarkable given the fact that a well depth is the only parameter assumed. This gives us some indication of how accurately we can make a potential well today. The number of electrons in a parabolic well in a given sample can be increased or decreased by illumination of the sample or by use of a surface gate electrode. Analysis of the resistance oscillations (in magnetic field) of the electron gas, as the number of electrons in the parabolic well is varied by either technique, show that the parabolic well fills at nearly constant 3D density, from zero thickness to thicknesses up to 2000 Å (*44*).

That the electrons are distributed uniformly in the parabolic well has been measured directly using capacitance-voltage profiling techniques, wherein the electron density versus depth profile is extracted from a measurement of the capacitance between a surface metal gate and the electron gas (which forms the other plate of the parallel-plate capacitor), at different gate-to-gas voltage biases. This simple measurement has been used to optimize MBE growth conditions to obtain more uniform and symmetric 3DEGs in parabolic wells (*45*).

These results suggest that the electron gas in a wide parabolic well is a promising candidate for the study of effects predicted for a 3DEG and of effects in the transitional regime from two to three-dimensionality. Experiments in this direction are under way by several research groups: for instance, there has been a study of the evolution of the fractional quantum Hall effect as the electron layer becomes thicker (*42*).

The parabolic wells also show striking optical effects. One interesting discovery occurred in the optical absorption of the electron plasma in the parabolic well (*46*). The plasma frequency of the 3DEG is calculated to be equal to the harmonic-oscillator spacing of the empty parabola. This frequency is in the far-infrared (FIR), typically 50 cm^{-1} (200-μm wavelength) for a density of 2 × 10^{16} cm^{-3}. It was discovered that, irrespective of the number of electrons in the well, the electron gas always absorbs at this bare harmonic-

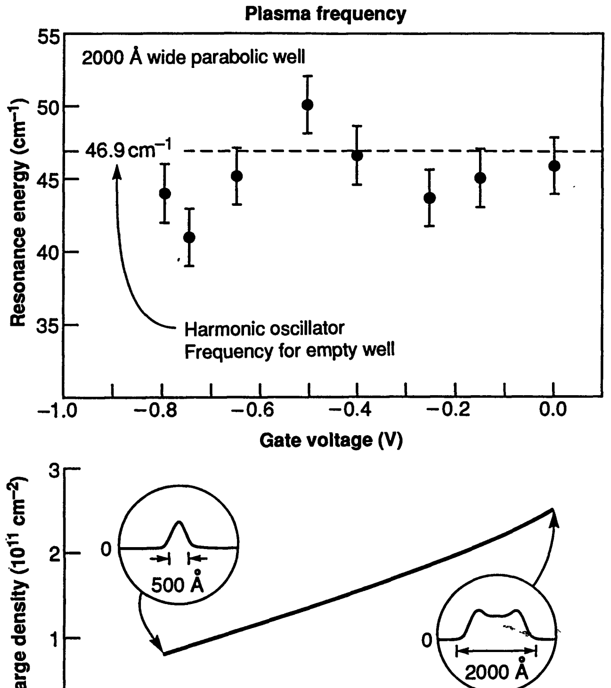

Fig. 12. Resonance energy of absorption of the three-dimensional electron versus gate voltage (top) shows absorption at the empty-well harmonic-oscillator frequency irrespective of the number of electrons in the well (changed by the gate voltage). This is a property unique to a ideal harmonic oscillator and is a consequence of the parabolic potential and the translational invariance of the electron-electron interaction. The bottom half shows how the number of electrons in the well is changed by the gate voltage. The insets depict how the increase in the number of electrons with more positive gate bias is accommodated by an increase in the thickness of the electron gas at constant 3D density.

oscillator frequency, as shown in Fig. 12 (*47*).

Recall that a single electron in a parabolic well partially filled with electrons sees a parabola with a flat bottom, the flattened region being proportional to the number of electrons in the well. Consequently, the energy spectrum of this individual electron is not the equally spaced one of a harmonic oscillator, but that of a flattened oscillator that is actually very close to a square-well spectrum. As the number of electrons is increased, the width of this approximate square well increases proportionately, with an attendant decrease in the energy spectrum spacing (for an infinitely deep square well, the energy spectrum changes inversely with the square of the well width). One would expect this change to be reflected in the FIR absorption of the 3DEG at different electron fillings. The observation that the gas always absorbs at one frequency suggests a more fundamental effect. It has been shown theoretically (*48*) that this is indeed a property unique to the ideal harmonic oscillator or parabolic well. The translational invariance of the electron-electron interaction (the fact that this interaction depends only on the relative distance between the two electrons) coupled with the quadratic form of the potential, when inserted in the Schrödinger equation, give the following general result: the motion of the center of mass of the 3DEG can be decoupled from the motion of the individual electron; as long as the wavelength is much larger than the thickness of the gas, the incident light simply grabs the entire cloud of electrons and oscillates it in unison. The maximum absorption is of course at the plasma or harmonic-oscillator frequency. The individual electron sees an approximate square potential well, but the ensemble of electrons sees the original parabola; applying a linear term to the parabolic potential with a gate bias does not change its second derivative and hence its plasma frequency.

This result is relevant to the case of quantum wires and boxes, where the optical absorption shows a similar independence of the number of electrons in the wire or box, a result which had puzzled researchers for a while. We now know this to be a consequence of the parabolic shape of the confining potential. Deviations from the parabolic potential, whether deliberate or unintentional, manifest themselves in the optical absorption spectra as additional structure and give clues to the modes of absorption of the individual electrons. Deviations from this generalized theorem for an ideal parabolic potential are being investigated in a systematic way in potential wells of different shapes, by several groups.

Thanks to computer-controlled MBE technology, pretty much any textbook potential well can be made. The square well and the parabolic well are the first examples. One could think of these potential wells as atoms, the shape and size of whose electrostatic potential can be controlled over a fairly large range in both distance and energy. By making these wells wide, one can access energy spectra in the FIR. Although we have so far discussed only wide symmetric (in the growth direction) wells, asymmetric wells also provide a rich field of study. For example, asymmetric wells have nonlinear optical responses. One group has recently observed second- and third-harmonic generation while subjecting electrons in a wide half-parabolic well to intense FIR radiation (*49*). This nonlinear response is predicted to develop into chaotic behavior in stronger driving electromagnetic fields (*50*).

Several groups are working on the properties of an electron gas in which the density is periodically modulated in the growth direction. Such a gas is realized by growing a modulation-doped wide (~2000 Å) parabolic well with a superimposed superlattice of shorter period (~200 Å) in the well: the slow parabolic potential ensures the uniform electron density, the superlattice then modulates this density by up to 100% (*51*). One technological application is a tunable FIR detector (*52*): in a specially shaped well, in which the local curvature varies with depth, a surface gate can be used to control the position of the center of the electron gas in the well and thereby tune the energy spectrum of the electrons, thus changing the wavelength of light at which these electrons have resonant absorption.

Performance limits for most such electronic devices as well as the chances of observing electron-electron interaction effects are enhanced to a large extent by the electron mobility. It appears that the factor that limits the electron mobility in the parabolic well structures may be a new type of scattering mechanism known as the size effect (*53*), related to a similar effect seen previously in thin metal films. Nonspecular or diffuse scattering of the electrons off the rough confining walls of the thick electron gas may be the dominant scattering mechanism in these structures. However, this is a current topic of research.

Background impurities and precise control of the mole-fraction profile of the graded $Al_xGa_{1-x}As$ are two important limitations to the growth of high-quality 3DEGs. Carbon atoms from residual gases in the vacuum system are the dominant ionized impurities in these MBE grown structures. Carbon is a shallow acceptor in GaAs, and is negatively charged in n-type material where the Fermi energy lies in the conduction band; these negatively charged acceptor ions act as strong scattering centers for electrons. Calculated fits to the mobilities for the best 3DEGs suggest carbon to be present in the alloy at the level of 2×10^{14} cm^{-3}, a reasonable number for a clean MBE machine. It is ultimately this density, too, that limits how dilute an electron gas can be achieved with this technique: a uniform negative background charge of 10^{14} to 10^{15} cm^{-3} ionized carbon acceptors will produce a parabolic potential of the opposite curvature to the design curvature, thus altering the desired parabola. The curvature can be controlled to within 10% in these MBE-grown graded alloys. Further improvements can be made with more precise computer control (faster clock), better oven temperature controllers (analog alloy), and using electric shutters instead of pneumatic ones in front of the ovens (digital alloy).

These limits are sufficiently broad that one can access a wide range of electron densities and distributions and a broad span of infrared energies with potential wells of controlled widths and shapes. These wells and gases constitute good candidates for the study of electron-electron interactions in 3DEGs (and in the transitional regime from 2D to 3D), nonlinear optical behavior and chaos in the FIR, and for the development of novel detectors and other FIR optical devices.

Summary and Conclusions

The rapid progress in two-dimensional electron structures is now being extended to semiconductor systems in which conduction electrons are constrained (at least partially) to free motion in one dimension, or are allowed, at least partially, free motion in the third dimension. The process of formation of these structures is intimately connected to epitaxial thin film crystal growth technology that enables the motion of atoms on surfaces to be governed by surface asperities as small as atomic thickness islands and terrace steps. What emerges from these studies is increased knowledge of the atomic processes of crystal growth and new information on the dynamics and the interactions of electrons under partial confinement in the quantum size regime. The technological promise that emerges from these studies is the discovery of new routes to enhanced quantum-based electronic and electro-optic devices and the discovery of new media for device structures in the submillimeter and far infrared regimes.

REFERENCES AND NOTES

1. For a review, see V. Narayanamurti, *Science* **235**, 1023 (1987).
2. For a review, see V. Narayanamurti, *Phys. Today* **37**, 24 (October 1984).
3. For a review, see B. I. Halperin, *Sci. Am.* **254**, 52 (April 1986); and *The Quantum*

Hall Effect, R. E. Prange and S. M. Girvin, Eds. (Springer-Verlag, New York, 1985).
4. B. J. van Wees *et al.*, *Phys. Rev. Lett.* **60**, 848 (1988).
5. For a review, see A. Y. Cho, *Thin Solid Films* **100**, 291 (1983); R. D. Dupuis, *Science* **226**, 623 (1984).
6. For a review, see H. L. Störmer, *Surf. Sci.* **132**, 519 (1983).
7. L. Pfeiffer, K. W. West, H. L. Störmer, K. W. Baldwin, *Appl. Phys. Lett.* **55**, 1888 (1989).
8. For a review, see J. P. Eisenstein and H. L. Stormer, *Science* **248**, 1510 (1990); H. L. Stormer and D. C. Tsui, *ibid.* **220**, 1241 (1983).
9. E. P. Wigner, *Phys. Rev.* **46**, 1002 (1934); for latest developments, see editorial by A. Khurana, *Phys. Today* **43**, 17 (December 1990).
10. For a review, see M. H. Brodsky, *Sci. Am.* **262**, 68 (February 1990).
11. For a review, see L. F. Eastman, *Phys. Today* **39**, 77 (October 1986).
12. For a review, see A. F. J. Levi, R. N. Nottenberg, Y. K. Chen, M. B. Panish, *ibid.* **43**, 58 (February 1990).
13. For a review, see Y. Suematsu, *ibid.* **38**, 32 (May 1985); D. S. Chemla, *ibid.*, p. 57.
14. H. Sakaki, *Jpn. J. Appl. Phys.* **19**, L735 (1980).
15. Y. Arakawa and H. Sakaki, *Appl. Phys. Lett.* **40**, 939 (1982).
16. J. Spector, H. L. Störmer, K. W. Baldwin, L. N. Pfeiffer, K. W. West, *ibid.* **58**, 263 (1991).
17. C. J. B. Ford *et al.*, *J. Phys.* **C21**, 1325 (1988).
18. H. L. Störmer, L. N. Pfeiffer, K. W. West, K. W. Baldwin, paper presented at the International Symposium on Nanostructures and Mesoscopic Systems, Santa Fe, NM, May 1991; L. Pfeiffer, *J. Cryst. Growth* **111**, 333 (1990).
19. E. Kapon, *Appl. Phys. Lett.* **55**, 2715 (1989).
20. P. M. Petroff, A. C. Gossard, W. Wiegmann, *ibid.* **45**, 620 (1984).
21. J. M. Gaines *et al.*, *J. Vac. Sci. Technol.* **B6**, 1378 (1988).
22. T. Fukui and H. Saito, *ibid.*, p. 1373; H. Yamaguchi and Y. Horikoshi, *Jpn. J. Appl. Phys.* **28**, 352 (1989).
23. S. A. Chalmers, H. Kroemer, A. C. Gossard, *Appl. Phys. Lett.* **57**, 1751 (1990).
24. M. S. Miller *et al.*, *J. Cryst. Growth* **111**, 323 (1991).
25. J. Motohisa, M. Tanaka, H. Sakaki, *Appl. Phys. Lett.* **55**, 1214 (1989).
26. K. Tsubaki, Y. Tokura, T. Fukui, H. Saito, N. Susa, *Electron. Lett.* **25**, 728 (1989).
27. T. Fukui, H. Saito, Y. Tokura, *Appl. Phys. Lett.* **55**, 1958 (1989).
28. S. A. Chalmers *et al.*, *ibid.*, p. 2491.
29. P. I. Cohen and P. R. Pukite, *J. Vac. Sci. Technol.* **A5**, 2027 (1987).
30. S. A. Chalmers, A. C. Gossard, P. M. Petroff, J. M. Gaines, H. Kroemer, *ibid.* **B7**, 1357 (1989).
31. P. R. Pukite, C. S. Lent, P. I. Cohen, *Surf. Sci.* **161**, 39 (1985).
32. J. H. Neave, P. J. Dobson, B. A. Joyce, J. Zhang, *Appl. Phys. Lett.* **47**, 100 (1985).
33. F. Briones, D. Golmayo, L. Gonzalez, A. Ruiz, *J. Cryst. Growth* **81**, 19 (1987); Y. Horikoshi, M. Kawashima, H. Yamaguchi, *Jpn. J. Appl. Phys.* **27**, 169 (1988).
34. S. A. Chalmers, A. C. Gossard, P. M. Petroff, H. Kroemer, *J. Vac. Sci. Technol.* **B8**, 431 (1990).
35. V. Celli and N. D. Mermin, *Phys. Rev.* **140**, A839 (1965).
36. The suggestion was made by A. C. Gossard and B. I. Halperin: see B. I. Halperin, *Jpn. J. Appl. Phys.* **26** (Suppl. 26-3), 1913 (1987).
37. M. Sundaram, A. C. Gossard, J. H. English, R. M. Westervelt, *Superlattices Microstruct.* **4**, 683 (1988).
38. These calculations solve both Poisson's equation and the Schrödinger wave equation with appropriate boundary conditions: see A. J. Rimberg and R. M. Westervelt, *Phys. Rev. B* **40**, 3970 (1989); T. Sajoto, J. Jo, H. P. Wei, M. Santos, M. Shayegan, *J. Vac. Sci. Technol.* **B7**, 311 (1989); M. P. Stopa and S. DasSarma, *Phys. Rev. B* **40**, 10048 (1989); A. Wixforth, M. Sundaram, K. Ensslin, J. H. English, A. C. Gossard, *Appl. Phys. Lett.* **56**, 454 (1990).
39. A. C. Gossard, *IEEE J. Quant. Electron.* **22**, 1649 (1986).
40. M. Sundaram, A. Wixforth, R. S. Geels, A. C. Gossard, J. H. English, *J. Vac. Sci. Technol.* **B9**, 1524 (1991).
41. M. Sundaram, A. C. Gossard, P. O. Holtz, *J. Appl. Phys.* **69**, 2375 (1991).
42. M. Shayegan, J. Jo, W. Suen, M. Santos, V. J. Goldman, *Phys. Rev. Lett.* **65**, 2916 (1990).
43. See, for example, P. F. Hopkins *et al.*, *Appl. Phys. Lett.* **57**, 2823 (1990).
44. E. G. Gwinn *et al.*, *Phys. Rev. B* **39**, 6260 (1989); T. Sajoto, J. Jo, M. Santos, M. Shayegan, *Appl. Phys. Lett.* **55**, 1430 (1989); K. Ensslin, M. Sundaram, A. Wixforth, J. H. English, A. C. Gossard, *Phys. Rev. B* **43**, 9988 (1991).
45. M. Sundaram and A. C. Gossard, in preparation.
46. K. Karraï, H. D. Drew, M. W. Lee, M. Shayegan, *Phys. Rev. B* **39**, 1426 (1989); K. Karraï, X. Ying, H. D. Drew, M. Shayegan, *ibid.* **40**, 12020 (1989).
47. A. Wixforth, M. Sundaram, K. Ensslin, J. H. English, A. C. Gossard, *ibid.* **43**, 10000 (1991).
48. L. Brey, N. F. Johnson, B. I. Halperin, *ibid.* **40**, 647 (1989).
49. W. W. Bewley *et al.*, in preparation.
50. M. Sherwin, in preparation.
51. J. Jo *et al.*, *Appl. Phys. Lett.* **57**, 2130 (1990); A. J. Rimberg *et al.*, paper presented at the International Symposium on Nanostructures and Mesoscopic Systems, Santa Fe, NM, May 1991.
52. J. Maserjian and A. C. Gossard, patent pending.
53. W. Walukiewicz, M. Sundaram, P. F. Hopkins, A. C. Gossard, R. M. Westervelt, in *Proceedings of the MRS Fall Meeting*, Boston, MA, 1990 (Materials Research Society, Pittsburgh, 1990).
54. We thank the following colleagues for discussions on matters pertaining to this article: P. M. Petroff, H. Kroemer, J. H. English, H. Weman, M. Miller, A. Wixforth, K. Ensslin, E. G. Gwinn, R. M. Westervelt, M. S. Sherwin, B. I. Halperin, A. J. Rimberg, and M. P. Stopa. Our thanks also to J. C. Yi for calculating and preparing Fig. 5, to S. Gidir and K. Campman for critical readings of the manuscript, and to D. J. McLarin for her skillful translation of some of the authors' ideas into lucid figures.

Microfabrication Techniques for Integrated Sensors and Microsystems

K. D. WISE AND K. NAJAFI

Integrated sensors and actuators are rapidly evolving to provide an important link between very large scale integrated circuits and nonelectronic monitoring and control applications ranging from biomedicine to automated manufacturing. As they continue to expand, entire microsystems merging electrical, mechanical, thermal, optical, magnetic, and perhaps chemical components should be possible on a common substrate.

THE DRAMATIC PROGRESS MADE BY MICROELECTRONICS over the past 30 years is obvious today in nearly all aspects of society. The number of transistors that can be successfully integrated on a single silicon chip is now over a million, and by the end of this decade that number is expected to increase another thousandfold. This progress will make very sophisticated control systems possible at low cost; however, the application of such systems in health care, biotechnology, industrial automation, automotive systems (including smart highways), and many consumer products will depend on the availability of low-cost, high-performance sensors and actuators with which to interface this control circuitry to a nonelectronic world. In response to increasing pressure from such system needs, during the past 30 years there has been an expanding effort toward sensor development based on the use of technologies similar to those used for integrated circuits.

The late 1960s saw the first efforts at adapting microfabrication techniques to the creation of miniature silicon sensors. After early temperature and pressure sensors, optical detector arrays were probably the first such devices to find their way into production, and today these devices are among the largest chips fabricated by the semiconductor industry, promising to revolutionize photography at

---

The authors are with the Center for Integrated Sensors and Circuits, The University of Michigan, Ann Arbor, MI 48109.